Article

Do Anatomical Differences of the Volar Rim of the Distal Radius Affect Implant Design? A Three-Dimensional Analysis of Its Anatomy and Need for Personalized Medicine

Hidemasa Yoneda *, Katsuyuki Iwatsuki, Masaomi Saeki, Michiro Yamamoto and Masahiro Tatebe

Department of Human Enhancement and Hand Surgery, Nagoya University, 65 Tsurumai-cho, Showa-ku, Nagoya 466-8560, Japan
* Correspondence: yoneda@med.nagoya-u.ac.jp; Tel.: +81-52-744-2957

Abstract: The distal radius, one of the frequent sites of upper extremity fractures, includes unique anatomy referred to as the volar rim. Few studies have addressed its interindividual differences. Additionally, implants for osteosynthesis must match the anatomical structures to prevent soft tissue invasion, but no implants have focused on that so far. In this study, three-dimensional surface models were created from CT images of 101 cases. Analysis of the distal radius, including the volar rim anatomy, was performed to design plates to minimize the discrepancy between the bone anatomy and the implant. The results showed that there were considerable interindividual differences in the morphology of the distal radius, particularly in the degree of palmar protrusion of the volar rim. A moderate correlation between the width of the distal radius and the shape of the volar rim was demonstrated. Considering that variations in plate width are available for treatment of normal distal radius fractures and that the shape of the volar rim changes in correlation with the width of the bone, we infer that simply adding volar rim shape information to the current variations should suffice in preventing complications. We conclude that individualized design according to the shape of the volar rim is unnecessary in fracture surgery.

Keywords: interindividual difference; distal radius fracture; tree-dimensional analysis; osteosynthesis with anatomical plate

1. Introduction

The anatomical morphology of bones is determined by various parameters such as height, weight, sex, age, nutritional status, and systemic diseases. The diaphysis is generally similar in shape [1], although there are variations in width and length [2], and the epiphysis and metaphysis near the joints show variations in three-dimensional shapes between individuals.

The volar rim, a characteristic morphology of the distal radius, is a structure with significant individual anatomical variation [2]. The volar rim projects palmarly, shifting the load-bearing axis from the lunate in the sagittal plane volarly, thus, transmitting the load of the hand to the elbow. This occurs largely through the palmar cortex, where the bone strength is high (Figure 1) [3]. The proximal part of the volar rim is covered with the pronator quadratus and the distal part is covered with fibrous tissue, forming the sliding floor of the flexor tendon located just above the rim [4,5].

The metaphyseal and epiphyseal areas of the radius, including this volar rim, are the sites where fractures frequently occur [6]. It is the area where strong forces are exerted during load transmission. Hence, a strong plate is used to maintain the restored position of the fracture. Since most plates used are ≥2 mm thick and are placed between the flexor tendon and bone where there is not much space, the influence on the flexor tendon and other soft tissues on the palmar side is substantial. Plates placed distally across the watershed line, the most prominent

part of the volar rim, and plates that protrude more than 2 mm palmarly in the sagittal plane have been reported to be at risk for flexor tendon injury [7,8].
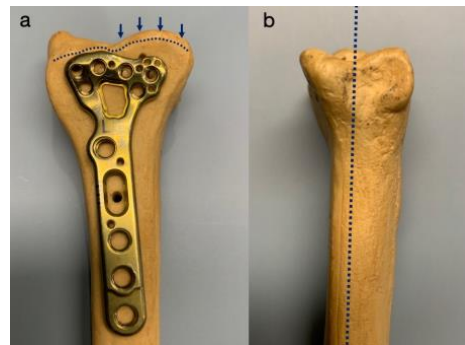
Figure 1. (**a**) Metaphyseal anatomy of the distal radius: The ulnar part of the distal radius, including the lunate fossa, constitutes the volar rim; the most prominent part is referred to as the watershed line (arrow). (**b**) In lateral view, the distal end of the bone, including the volar rim, is shifted palmarly, and the load from the lunate is mainly received by the palmar cortex of the bone (dotted line) rather than the center of the bony axis.

In recent years, plates designed to have a smaller palmar protrusion than the volar rim protrusion and ones with three-dimensional bending to match the shape of the volar rim have been introduced to reduce this effect on the palmar soft tissue (Figure 2) [4]. However, the only option for plates for osteosynthesis is bone width, which does not correspond to the anatomical variation of the volar rim.
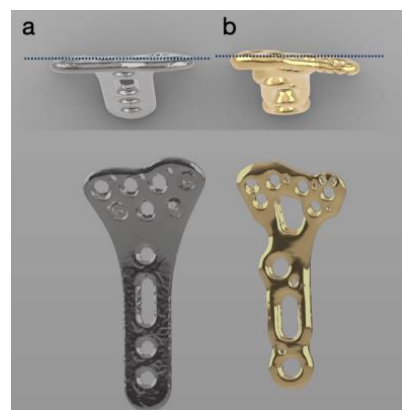
Figure 2. A plate with flat distal portion (**a**) and a plate bent to match the rim shape (**b**).

Few studies have investigated individual variations in the volar rim. Sometimes plates with shapes significantly different from the anatomical shape are placed and can cause the rupture of the flexor tendon [2,9–12]. In this study, we examined three-dimensional variations in the shape of the volar rim. Additionally, we discussed whether a personalized implant shape design corresponding to the individual morphology of the volar rim is necessary for the treatment of fractures.

2. Materials and Methods

This study was performed after the approval of the institutional review board of our hospital. The patient age and gender were extracted from the medical records. We used computed tomography (CT) images of the wrist taken at our hospital over the past 10 years. The CT scanner was an Acquilion (Canon Medical Systems, Tokyo, Japan) and the image data were outputted with a slice thickness of 0.4 mm, segmented using Mimics 21.0 (Materialise, Leuven, Belgium), and then again outputted as a 3D surface model (Standard

Triangulated Language, STL file) of the bone. Patients with inflammatory diseases such as rheumatoid arthritis or osteoarthritis of the hand and patients with a history of fractures were excluded from the analysis. Patients younger than 20 years of age were excluded. The surface models with less than 7 cm were excluded.

Measurements were performed using the 3D analysis software Rhinoceros 6.0 (Robert McNeel & Associates, Seattle, WA, USA). Concentric circles were created at 4 cm and 6 cm from the articular surface and the line connecting the centers of the circles was defined as the Z-axis (Figure 3). If the Z-axis was apparently different from the long axis of the radius, the Z-axis was adjusted to match its long axis. The distal radioulnar joint was identified in a cross-section perpendicular to the Z-axis and included the most proximal part of the radiocarpal joint. In the joint, the X-axis was defined as the line connecting the two points on the palmar and dorsal sides of the articular surface. The Y-axis is the axis perpendicular to it in the cross-section. The planes perpendicular to the X-, Y-, and Z-axes were defined as coronal, sagittal, and transverse planes, respectively.
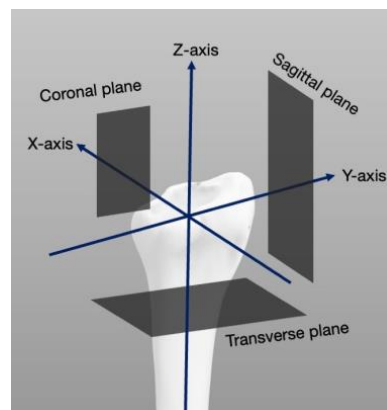
Figure 3. Schemas of measurement axes (X-, Y-, and Z-axes) and coronal, sagittal, and transverse planes.

The tangent line of the bone cortex at the most prominent part of the palmar side in a transverse section, 4 cm from the articular surface, was set as the U-axis (Figure 4). The T-axis was then defined as a straight line passing through the most prominent part of the palmar volar rim and the prominent part of the palmar cortex of the scaphoid fossa in a transverse section passing through the most prominent part of the volar rim (Figure 4). The angle between the T-axis and the U-axis was measured as the angle of rotation of the metaphysis relative to the diaphysis [13].
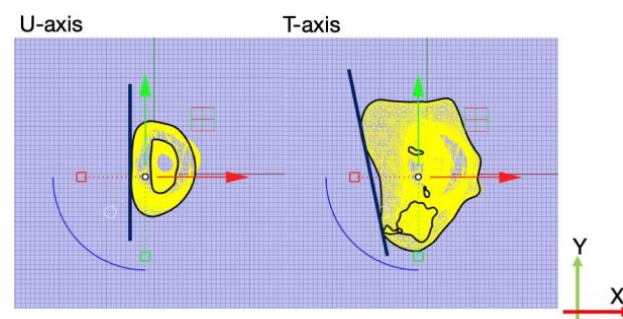
Figure 4. Measuring of the angle of rotation in the metaphysis: The angle of rotation of the metaphysis was measured as the angle between the tangent line (U-axis) of the most prominent part of the palmar cortex in a transverse section, 4 cm from the articular surface, and the line connecting the volar rim at its central level of it and the prominent part of the palmar cortex of the scaphoid fossa (T-axis).

Measurements for the quantitative analyses were performed in the transverse and sagittal planes. In the transverse plane, we measured the angle of metaphysis rotation as

described above and the bone width of the radius in the S plane. We also measured the angle between the Y-axis and the tangent line of the most prominent part (axial angle) and the prominent distance from the concave surface of the palmar side to the most prominent point of the volar rim (Figure 5). In the sagittal plane, as per the method of Yoneda et al., the angle of the inflection point on the cortex was taken as the teardrop inclination angle and the distance to the inflection point as the teardrop length (Figure 6) [2]. The teardrop inclination angle cannot be used for designing plates because the position of the inflection point varies in each case (Figure 7). To design the plate, the distance between the watershed line and inflection point was set to the average of the teardrop length and the sagittal angle, which corresponds to the bending angle of the plate in the sagittal plane, was measured. Finally, the transverse section was tilted based on the sagittal angle and the axial angle was measured as the modified axial angle.
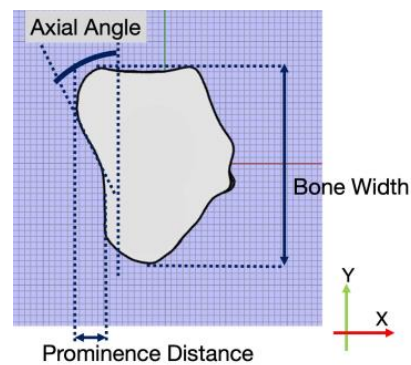
Figure 5. Measurements of bone width, axial angle, and prominence distance: They were measured in transverse section including the base of the subchondral bone forming the radiocarpal joint. The bone width was the longest length parallel to Y-axis and the axial angle was the angle between the Y-axis and the tangent line through the palmar projection of the volar rim. The prominence distance was the protrusion of the lunate fossa relative to the scaphoid fossa, measured on the X-axis.
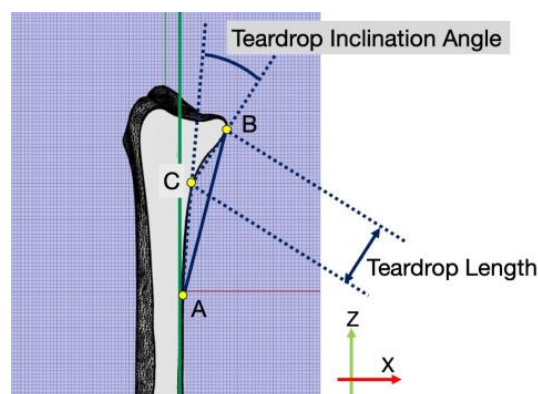
Figure 6. Measurement of teardrop inclination angle and teardrop length: In the sagittal plane passing through the center of the volar rim, draw a shaft line through the palmar aspect of the radius and parallel to the bony axis. Drag a line segment AB connecting point A, where the palmar cortex separates from the shaft line, and the inflection point B of the cortex. Then, determine the point C on the ulnar cortex farthest from AB. The teardrop inclination angle is measured as the external angle created by the two lines, AC and BC, and the length of BC is the teardrop length.
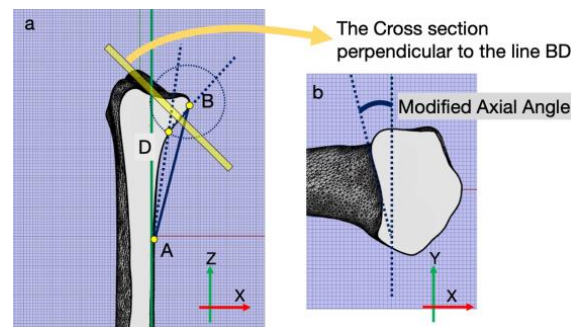
Figure 7. Measurement of sagittal angle and modified axial angle: (**a**) The same method was used to determine points A and B, as in Figure 6. Point D on the palmar cortex is plotted in the sagittal plane so that the length of D is the determined value of the teardrop length. The angle between AD and BD is measured as the sagittal angle. (**b**) The plane perpendicular to BD is the modified transverse plane and the axial angle is measured on that plane.

3. Results

The number of cases for image analysis was 108, of which seven were excluded based on the exclusion criteria. Ultimately, surface models for the analysis were created using CT images of 101 cases (50 males and 51 females). A summary of the quantitative measurements is shown in Table 1. In the transverse section, the bone width averaged 27.1 mm (SD 2.8), the rotation angle averaged 8.8° (SD 6.0), and the axial angle was 16.4 (SD 8.3). The mean teardrop inclination angle was 22.8 (SD 6.2) and the mean teardrop length was 12.1 (SD 2.7). Then, when the teardrop length was set to 12 mm, the average sagittal angle was 26.6° (SD 6.5) and the modified axial angle was 12.0° (SD 2.8). The coefficients of variation were more than 0.2 except for the bone width, suggesting individual differences in the anatomical morphology of the radius.

Table 1. Summary of the quantitative measurements.

	Average $\pm$ SD (CV)		
	Male	**Female**	**Total**
Number of patients	50	51	101
Age [y]	58.9 ± 14.0	61.1 ± 12.0	60.0 ± 13.0
Bone width [mm] *	29.1 ± 1.6 (0.05)	25.2 ± 2.3 (0.09)	27.1 ± 2.8 (0.10)
Rotation of metaphysis [°]	8.8 ± 6.1 (0.69)	8.8 ± 5.9 (0.67)	8.8 ± 6.0 (0.68)
Teardrop inclination angle [°]	25.2 ± 4.7 (0.19)	20.4 ± 6.7 (0.33)	22.8 ± 6.2 (0.27)
Teardrop length [mm] *	11.7 ± 2.7 (0.23)	12.5 ± 2.7 (0.22)	12.1 ± 2.7 (0.23)
Sagittal angle [°] *	28.9 ± 4.5 (0.16)	24.4 ± 7.4 (0.30)	26.6 ± 6.5 (0.24)
Prominence distance [mm] *	6.2 ± 1.4 (0.47)	5.3 ± 1.6 (0.30)	5.76 ± 1.6 (0.27)
Axial angle [°]	17.9 ± 8.4 (0.22)	14.9 ± 8.0 (0.10)	16.4 ± 8.3 (0.51)
Modified axial angle [°]	12.0 ± 2.9 (0.24)	11.8 ± 2.7 (0.23)	12.0 ± 2.8 (0.23)

SD, standard deviation; CV, coefficient of variation. * Significant difference between males and females by Welch test ($p < 0.05$).

Among the measured items, the mean values of bone width, teardrop inclination angle, sagittal angle, and prominence distance differed between males and females (Table 1). No correlation with age was observed for any of the items. There was no correlation between bone width and angle of rotation, but moderate correlations were found between the sagittal angle, teardrop inclination angle, and axial angle (Table 2). Moderate correlations were also observed between modified axial angles.

Table 2. Correlations between measured parameters.

Parameters	Coefficient of Correlation	
Age—Bone width	−0.27	
Age—Rotation of metaphysis	−0.18	
Age—Teardrop inclination angle	−0.13	
Age—Teardrop length	0.09	
Age—Sagittal angle	−0.09	
Age—Axial angle	−0.23	
Age—Prominence distance	−0.28	
Age—Modified axial angle	−0.19	
Bone width—Rotation of metaphysis	0.16	
Bone width—Sagittal angle	0.46	*
Sagittal angle—Axial angle	0.53	*
Teardrop inclination angle—Axial angle	0.53	*
Sagittal angle—Modified axial angle	0.46	*
Teardrop inclination angle—Modified axial angle	0.44	*

* $p < 0.05$.

The subgroup analysis was performed by dividing all models into three groups based on the bone width: lower 1/3 (range from 21.3 to 25.6 mm; small), middle 1/3 (range from 25.7 to 28.0 mm; medium), and upper 1/3 (range from 28.1 to 35.3 mm; large) with 33, 35, and 33 cases in the small, medium, and large groups, respectively. In the small and medium groups, a moderate correlation was observed between the sagittal and modified axial angles. However, the correlation between the sagittal and modified axial angles was lower in the large group (Figure 8). These results indicate that in bones with moderate or smaller widths, it is possible to create implants that match the shape of the rim. This can be achieved by preparing several variations correlating the angle of bending in the sagittal plane with the angle in the transverse plane. Conversely, in bones with large widths, the variation of the volar rim in the transverse and sagittal planes is large, causing it to be difficult to design an implant matching the shape of the volar rim even if multiple variations can be prepared. Possibly, the ulnar distal part of the plate should be adjustable to match the anatomy of the individual volar rim.
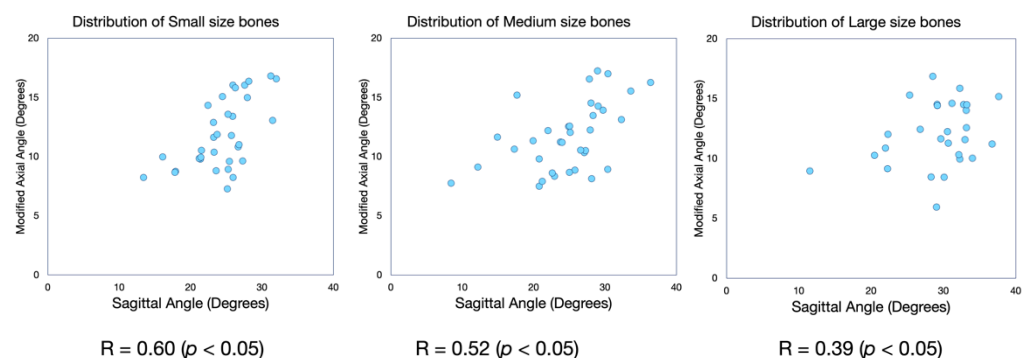
Figure 8. Distribution of sagittal angle and modified axial angle in subgroup analysis.

4. Discussion

It is widely known that there are individual differences in the morphology of the volar rim that cannot be explained by gender, extension, or weight alone. Several quantitative reports have been published previously and implants have been developed based on these findings. Oura et al. found that the amount of palmar protrusion in the transverse section was maximized at 4–6 mm from the articular surface, corresponding to the volar rim area [13]. In an analysis of reconstructed images from CT images, Andarmahr et al. found that the volar rim protrusion averaged 6 mm in the sagittal plane and Yoneda et al. showed that the angle between the protruding portion in the sagittal plane and the bone axis was

29° [2,14]. Kwon et al. found that the slope of the volar rim in the sagittal plane is steeper in males than in females [9].

A variation in the amount of palmar projection of the volar rim is one of the factors that concerns surgeons during plate placement in distal radius fracture surgery. Suppose the palmar protrusion of the volar rim is extensive, in that case, the plate may protrude similarly, preventing reconstruction of the flexor tendon gliding floor, and cause irritation of the flexor tendons or the median nerve. Therefore, the current treatment consensus requires that the plate not be placed distal to the watershed line and that it should not protrude palmarly more than 2 mm beyond the palmar aspect of the volar rim in the sagittal plane. Although it is desirable to use implants designed for individual geometries, current fracture implants offer only options for width and length and few implants offer possibilities for the bending angle of the plate that considers the shape of the volar rim.

The use of angularly stable locking plates to assemble fractures using implants as templates has become common [15,16]. In contrast, osteotomies for malunions are being performed based on preoperative planning using 3D image analysis technology and implants have been introduced that are placed according to the individual geometry of the osteotomy [17]. For fracture treatment, the use of implants that match the individual anatomy is ideal because a large discrepancy between the anatomical shape to be restored and the shape of the plate can cause malunion. However, because fractures are operated on a semi-emergency basis, individualized treatment is usually not feasible. Therefore, it is realistic to prepare multiple variations of implants and semi-customize the selection at the time of surgery and it is necessary to clarify the shape of the implant to accommodate these variations.

This study exhibited that gender is a factor that can affect bone width and volar rim anatomy, but age is unrelated to it. Previous studies have reported an effect of gender on fracture plate fit and the findings of this study support this [18]. The sagittal and transverse protrusions of the volar rim are moderately correlated. Furthermore, the individual differences in volar rim shape were found to be significant for bones with large widths. These results suggest that for bones with bone widths approximately less than 28 mm, plates should be designed with bending angles in the transverse plane that correlate to the bending angle in the sagittal plane. In bones with large bone widths, the variation in the shape of the volar rim tends to be significant, so it is desirable to be able to individually adjust the shape of the plate to match the rim shape. We conclude that for most bones, a plate with minimal soft tissue invasion can be designed using the above information and that custom-made plates are not necessary for treating fractures.

Next, the same investigation should be performed for other metaphyseal sites, such as distal femoral, proximal tibia, and distal tibia fractures. Similar to the distal radius fractures, the fixation strength of fractures with implants has been generally satisfactory in these sites and the next issue to be solved is the prevention of soft tissue problems caused by discrepancies between bone anatomy and implant shape [19,20]. The need for semi-custom implant design for fracture treatment based on individual bone anatomy for the treatment of any epiphyseal fractures needs to be clarified as well.

5. Limitation

This study had some limitations. First, because the analysis was limited to the bones of Asians, the external validity of the results for other races is uncertain. Second, the number of bones examined was small and multivariate analysis could not be performed to identify the factors affecting shape. Third, the thickness of the plate was not considered in this study, so the invasion of soft tissue could not be accurately predicted.

6. Conclusions

In conclusion, there are individual differences in the shape of the radius epiphysis and for bones of moderate or lower grade the size of the volar rim has a moderate correlation with the bone width in both the sagittal and transverse planes. As per the results of this study, we propose the development of several types of semi-custom plates with correlated

sagittal and transverse bending angles. This allows for osteosynthesis with minimal soft tissue invasion while accommodating for the anatomical diversity of the volar rim.

References

1. Gosman, J.H.; Hubbell, Z.R.; Shaw, C.N.; Ryan, T.M. Development of Cortical Bone Geometry in the Human Femoral and Tibial Diaphysis. *Anat. Rec.* **2013**, *296*, 774–787. [CrossRef] [PubMed]
2. Yoneda, H.; Iwatsuki, K.; Hara, T.; Kurimoto, S.; Yamamoto, M.; Hirata, H. Interindividual anatomical variations affect the plate-to-bone fit during osteosynthesis of distal radius fractures. *J. Orthop. Res.* **2016**, *34*, 953–960. [CrossRef]
3. Heifner, J.J.; Orbay, J.L. Assessment and Management of Acute Volar Rim Fractures. *J. Wrist Surg.* **2022**, *11*, 214–218. [CrossRef]
4. Limthongthang, R.; Bachoura, A.; Jacoby, S.M.; Osterman, A.L. Distal Radius Volar Locking Plate Design and Associated Vulnerability of the Flexor Pollicis Longus. *J. Hand Surg.* **2014**, *39*, 852–860. [CrossRef] [PubMed]
5. Imatani, J.; Akita, K.; Yamaguchi, K.; Shimizu, H.; Kondou, H.; Ozaki, T. An Anatomical Study of the Watershed Line on the Volar, Distal Aspect of the Radius: Implications for Plate Placement and Avoidance of Tendon Ruptures. *J. Hand Surg.* **2012**, *37*, 1550–1554. [CrossRef] [PubMed]
6. Baumbach, S.F.; Schmidt, R.; Varga, P.; Heinz, T.; Vécsei, V.; Zysset, P.K. Where is the distal fracture line location of dorsally displaced distal radius fractures? *J. Orthop. Res.* **2011**, *29*, 489–494. [CrossRef] [PubMed]
7. Soong, M.; Earp, B.E.; Bishop, G.; Leung, A.; Blazar, P. Volar Locking Plate Implant Prominence and Flexor Tendon Rupture. *J. Bone Jt. Surg.* **2011**, *93*, 328–335. [CrossRef] [PubMed]
8. Kitay, A.; Swanstrom, M.; Schreiber, J.J.; Carlson, M.G.; Nguyen, J.T.; Weiland, A.J.; Daluiski, A. Volar Plate Position and Flexor Tendon Rupture Following Distal Radius Fracture Fixation. *J. Hand Surg.* **2013**, *38*, 1091–1096. [CrossRef]
9. Kwon, B.C.; Lee, J.K.; Lee, S.Y.; Hwang, J.Y.; Seo, J.-H. Morphometric Variations in the Volar Aspect of the Distal Radius. *Clin. Orthop. Surg.* **2018**, *10*, 462–467. [CrossRef] [PubMed]
10. Imatani, J.; Akita, K. Volar Distal Radius Anatomy Applied to the Treatment of Distal Radius Fracture. *J. Wrist Surg.* **2017**, *6*, 174–177. [CrossRef]
11. Mishra, P.K.; Nagar, M.; Gaur, S.C.; Gupta, A. Morphometry of distal end radius in the Indian population: A radiological study. *Indian J. Orthop.* **2016**, *50*, 610–615. [CrossRef]
12. Kumar, A.; Passey, J.; Chouhan, D.; Saini, M.; Narang, A. CT Based Characterization of Volar Surface of Distal Radius: Can an Ideal Volar Plate for Fixation of Distal Radial Fractures be Designed? *J. Hand Surg. (Asian-Pac. Vol.)* **2021**, *26*, 77–83. [CrossRef] [PubMed]
13. Oura, K.; Oka, K.; Kawanishi, Y.; Sugamoto, K.; Yoshikawa, H.; Murase, T. Volar morphology of the distal radius in axial planes: A quantitative analysis. *J. Orthop. Res.* **2015**, *33*, 496–503. [CrossRef] [PubMed]
14. Andermahr, J.; Lozano-Calderon, S.; Trafton, T.; Crisco, J.J.; Ring, D. The Volar Extension of the Lunate Facet of the Distal Radius: A Quantitative Anatomic Study. *J. Hand Surg.* **2006**, *31*, 892–895. [CrossRef] [PubMed]
15. Toros, T.; Sügün, T.S.; Özaksar, K. Complications of distal radius locking plates. *Injury* **2013**, *44*, 336–339. [CrossRef] [PubMed]
16. Buzzell, J.E.; Weikert, D.R.; Watson, J.T.; Lee, D.H. Precontoured Fixed-Angle Volar Distal Radius Plates: A Comparison of Anatomic Fit. *J. Hand Surg.* **2008**, *33*, 1144–1152. [CrossRef] [PubMed]
17. Oka, K.; Shigi, A.; Tanaka, H.; Moritomo, H.; Arimitsu, S.; Murase, T. Intra-articular corrective osteotomy for intra-articular malunion of distal radius fracture using three-dimensional surgical computer simulation and patient-matched instrument. *J. Orthop. Sci.* **2020**, *25*, 847–853. [CrossRef] [PubMed]

18. Perrin, M.; Badre, A.; Suh, N.; Lalone, E.A. Analysis of Three-Dimensional Anatomical Variance and Fit of the Distal Radius to Current Volar Locking Plate Designs. *J. Hand Surg. Glob. Online* **2020**, *2*, 277–285. [CrossRef] [PubMed]
19. Mb, O.; Aksan, T.; Ertekin, C.; Tezcan, M. Coverage of exposed bone and hardware of the medial malleolus with tibialis posterior artery perforator flap after ankle fracture surgery complications. *Int. Wound J.* **2020**, *17*, 429–435. [CrossRef] [PubMed]
20. Chou, Y.-C.; Wu, C.-C.; Chan, Y.-S.; Chang, C.-H.; Hsu, Y.-H.; Huang, Y.-C. Medial Gastrocnemius Muscle Flap for Treating Wound Complications After Double-Plate Fixation via Two-Incision Approach for Complex Tibial Plateau Fractures. *J. Trauma Acute Care Surg.* **2010**, *68*, 138–145. [CrossRef] [PubMed]